Mesostructural changes in cellulose within wood cell wall upon hydrothermal treatment at 200 °C

Tomoko Kuribayashi, Yu Ogawa, I. Morfin, Yuji Matsumoto, Yoshiharu Nishiyama

Mesostructural changes in cellulose within wood cell wall upon hydrothermal treatment at 200 °C

Tomoko Kuribayashi [a, b, c, *], Yu Ogawa [d], Isabelle Morfin [e], Yuji Matsumoto [a], Yoshiharu Nishiyama [d, *]

[a] Graduate School of Agricultural and Life Sciences, The University of Tokyo, Yayoi 1-1-1, Bunkyo-Ku, 113-8657 Tokyo, Japan

[b] Department of Bioproducts and Biosystems, Aalto university, Vuorimiehentie 1, 02150 Espoo, Finland

[c] Department of Food and Nutrition, University of Helsinki, P.O. Box 66, 00014 Helsinki, Finland

[d] Univ. Grenoble Alpes, CNRS, CERMAV, 38000 Grenoble, France

[e] Univ. Grenoble Alpes, CNRS, LiPhy, 38000 Grenoble, France

*Corresponding authors:

T. Kuribayashi, tomoko.kuribayashi@aalto.fi

Y. Nishiyama, yoshiharu.nishiyama@cermav.cnrs.fr

Abstract

Hydrothermal treatment between 150 °C and 230 °C is widely used in wood processing, from the steam treatment of timber for better dimensional stability and durability to the pretreatment for enzymatic saccharification and chemical pulping. Understanding the ultrastructural changes of wood cell walls through hydrothermal treatments is crucial for controlling and optimizing these hydrothermal treatment-based processes. Here, we studied the ultrastructure of wood cell walls of 24 hardwood species using simultaneous small- and wide-angle X-ray scattering measurements before and after the hydrothermal

treatment at 200 °C. Most hardwoods show similar equatorial scattering features, representing the structure in the cross-section of the cell walls. In a water-saturated native state, there is a prominent correlation peak between 0.1 and 0.2 $Å^{-1}$ and a second peak between 0.2 and 0.4 $Å^{-1}$. The hydrothermal treatment above 160 ˚C drastically altered the structure at this nanometric scale: the two native correlation peaks disappeared, coincident with a buildup of a correlation peak in the 0.03-0.04 $Å^{-1}$ range. The hydrothermal treatment likely removed the cell wall matrix component between the microfibrils through autohydrolysis and phase separation, leading to the collapse of microfibrils with each other in the normal wood. In cellulose-rich cell walls, such as the G-layer in tension wood, cellulose microfibrils are already collated in the native state.

Keywords: Wood; Cellulose microfibril; Mesostructure; X-ray scattering; Hydrothermal treatment; Co-crystallization

Introduction

Thermal treatment between 150°C and 230°C with moisture is commonly used in timber processing. Heat steam treatment decreases wood's equilibrium moisture content, improving dimensional stability and durability (Kocaefe et al. 2015; Sandberg and Kutnar 2016). Hydrothermal treatment with excess water causes partial hydrolysis of the hemicelluloses that generates water-soluble saccharides and increases the specific surface area of the wood (Garrote et al. 1999). Such effects are helpful in the pretreatment of woody biomass for saccharification and chemical pulping (Garrote et al. 1999; Nitsos et al. 2013, 2016; Romani et al. 2010; Wojtasz-Mucha et al. 2017). The ultrastructural changes of wood cell walls by hydrothermal treatments are thus an

important parameter.

X-ray scattering can probe the structural features over wide length scales, typically from angstroms to a few hundred nanometers, without special sample preparation, which makes it a suitable analytical tool for structural investigations of plant cell walls (Jakob et al. 1994, 1996; Fernandes et al. 2011; Penttilä et al. 2019). Small- (SAXS) and wide-angle X-ray scattering (WAXS) have been used to study the structural evolutions of fully hydrated aspen (Nishiyama et al. 2014) and bagasse (Driemeier et al. 2015) during hydrothermal treatments. These studies found several common structural changes, such as co-crystallization of cellulose and phase separation of the cell wall matrix component (Nishiyama et al. 2014; Kuribayashi et al. 2016). We extended this study to broader spectrum wood samples, including 24 hardwood species before and after hydrothermal treatment at 200 °C for 2 hours using simultaneous S/WAXS measurements.

Experimental

Materials

Green beech (*Fagus crenata*) was harvested from The University of Tokyo Chichibu Forest (Saitama, Japan). Blocks (dimensions: 13 mm×13 mm×60 mm in the direction of tangential (T), radial (R), and longitudinal (L), respectively) were sawn out from the mature sapwood and stored in water with sodium azide at 4˚C.

Air-dried 24 hardwood specimens are summarized in Table 1. These were harvested in Japan and kindly provided by the Research Institute for Sustainable Humanosphere (RISH), Kyoto University, Japan.

Table 1. A list of wood specimens and their moisture contents

No.	Scientific name	Common name	Mc [%] (1)		
			Air Dry	Wet	
			Untreated	Untreated	Thermal treated
1	*Acer* sp.	Maple	7	121	123
2	*Aesculus turbinata*	Japanese horse-chestnut	8	123	128
3	*Aphananthe aspera*	Muku tree	8	82	87
4	*Castanea crenata*	Japanese chestnut	8	117	110
5	*Castanopsis* sp.	Chinquapin	8	116	105
6	*Celtis sinensis*	Chinese hackberry (2)	7	142	130
7	*Cercidiphyllum japonicum*	Katsura	7	139	139
8	*Cinnamomum camphora*	Camphor tree	7	108	128
9	*Cleyera japonica*	Japanese cleyra	6	187	183
10	*Diospyros kaki*	Japanese persimmon	6	94	97
11	*Distylium racemosum*	Isu tree	10	98	97
12	*Firmiana simplex*	Chinese parasol tree	7	90	86
13	*Fraxinus mandshurica*	Manchurian ash	6	133	149
14	*Ilex integra*	Mochi tree	6	82	88
15	*Kalopanax septemlobus*	Castor aralia (2)	6	135	143
16	*Liriodendron tulipifera*	Yellow poplar	7	141	154
17	*Magnolia obovata*	Japanese bigleaf magnolia	9	114	148
18	*Morus* sp.	Mulberry	7	135	130
19	*Quercus* sp.	Oak	9	110	83
20	*Quercus acutissima*	Sawtooth oak	9	85	83
21	*Quercus crispula*	Mizunara	7	100	97
22	*Styphnolobium japonicum*	Japanese pagoda tree	6	96	98
23	*Ulmus davidiana*	David elm	8	193	209
24	*Zelkova serrata*	Japanese elm	9	120	116

(1) Mc [%] = Dry basis moisture content. (2) Tension wood.

Preparation of water-swollen wood samples

Cylindrical samples with about 2 mm diameter and 10 mm length in fiber direction were cut out from the air-dried wood blocks. Specimens were cropped from the part without visible large vessel pores and medullary rays. Deionized water was soaked in the samples by vacuum pressure impregnation until the sample weight did not increase. The dry-basis moisture content of water-saturated samples was estimated as follows. A part of air-dried samples was dried overnight in an oven at 105 °C to obtain the dry weight. We calculated the equilibrium moisture contents of water-saturated samples in the ambient condition and considered it to be the same for each wood species. Moisture

contents in the water saturated samples were estimated taking into account the equilibrium moisture contents and weight gain by water impregnation. The calculated moisture contents in air-dried and water-saturated states were summarized in Table 1. Immediately after weighing the water-saturated sample, each wet sample was sealed into a glass tube (3 mm outer diameter, 200 μm wall thickness).

Hydrothermal treatment

The glass tubes containing a wood sample and a drop of water for pressure regulation were placed in a 30 ml pressure vessel and heat-treated in an oil bath at 200 °C for 2 hours. The partial water vapor pressure during hydrothermal treatment is 1.6 MPa according to the Tetens approximation formula. After the treatment, the vessel was quenched with ice.

Simultaneous SAXS and WAXS measurement

X-ray scattering experiments were performed at the D2AM beamline of the European Synchrotron Radiation Facility (ESRF). The tubes containing samples were probed with a monochromatic X-ray of 18 keV ($\lambda = 0.6889$ Å) before and after the hydrothermal treatment. The incident beam was orthogonal to the sample tubes. The scattering intensity was measured using two-dimensional pixel detection (XPAD-WOS and D5). Two sets of camera distances, D5 at 2.2 m and WOS at 32 cm or D5 at 1 m and WOS at 12 cm were used to cover a scattering vector range of q ($2\pi/d$) = 0.005 to 6 $Å^{-1}$.

In-situ X-ray scattering measurement over the thermal treatment

We used an aluminum block with 3 mm perforations to fit sample tubes and holes for incoming X-rays and scattered X-rays at D2AM beamline (ESRF). The temperature was regulated by using a heater regulated by a Eurotherm temperature controller.

Sample tubes containing green wood and wood with moisture content of 0-30 % were sealed by flame and placed in the sample holder. The samples were first heated from 25 °C to 80 °C, and the temperature was elevated stepwise by 10 °C with 10 minutes of holding time. After reaching 200 °C, the temperature was kept for 2 hours, then cooled to 23 °C by heat dissipation. The X-ray energy was 16 keV (λ = 0.775 Å). The scattered X-rays were recorded on a fiber optic coupled CCD camera. The experiment was repeated twice with two detector distances, 1.6 m and 16 cm, to cover a q range from 0.03 to 2 $Å^{-1}$.

Data analysis

The beam center and the detector positions were refined using PyFAI (Ashiotis et al. 2015) software using silver behenate and Cr_2O_3 diluted with microcrystalline cellulose powder in the same sample tube as the calibrant. The data were scaled by transmission intensity and remapped into polar coordinates. The intensity of the overlapping region was used to scale the two data sets measured at different detector distances and merged into one figure. The isotropic scattering level was estimated for each scattering angle by averaging 10 % of pixels of the lowest intensities. For the in-situ experiment data, the azimuthal intensity distributions were fitted with a constant and a Gaussian function for each scattering angle to separate the isotropic and the equatorial (anisotropic) contributions (Nishiyama et al. 2014).

Results and discussion

Changes in the scattering profile of anisotropic components

Examples of scattering patterns obtained from *Quercus* sp. are shown in Fig. 1. The untreated and treated wood show anisotropic scattering features over the whole q range: SAXS-1 and 2 show a streak in the equatorial direction (Fig. 1(a)), while WAXS-1 and

2 show fiber diffraction patterns where cellulose is oriented along the long axis of wood (Fig. 1(b)). The scattering profile of equatorial components of *Quercus* sp. is shown in Fig. 1(c), where q×I is plotted as a function of q, where I is an intensity count at a given q. Multiplying by q is equivalent to making an abstraction of the misalignment of cylindrically symmetric structure and extracting the power spectrum of the electron density of the cross-section.

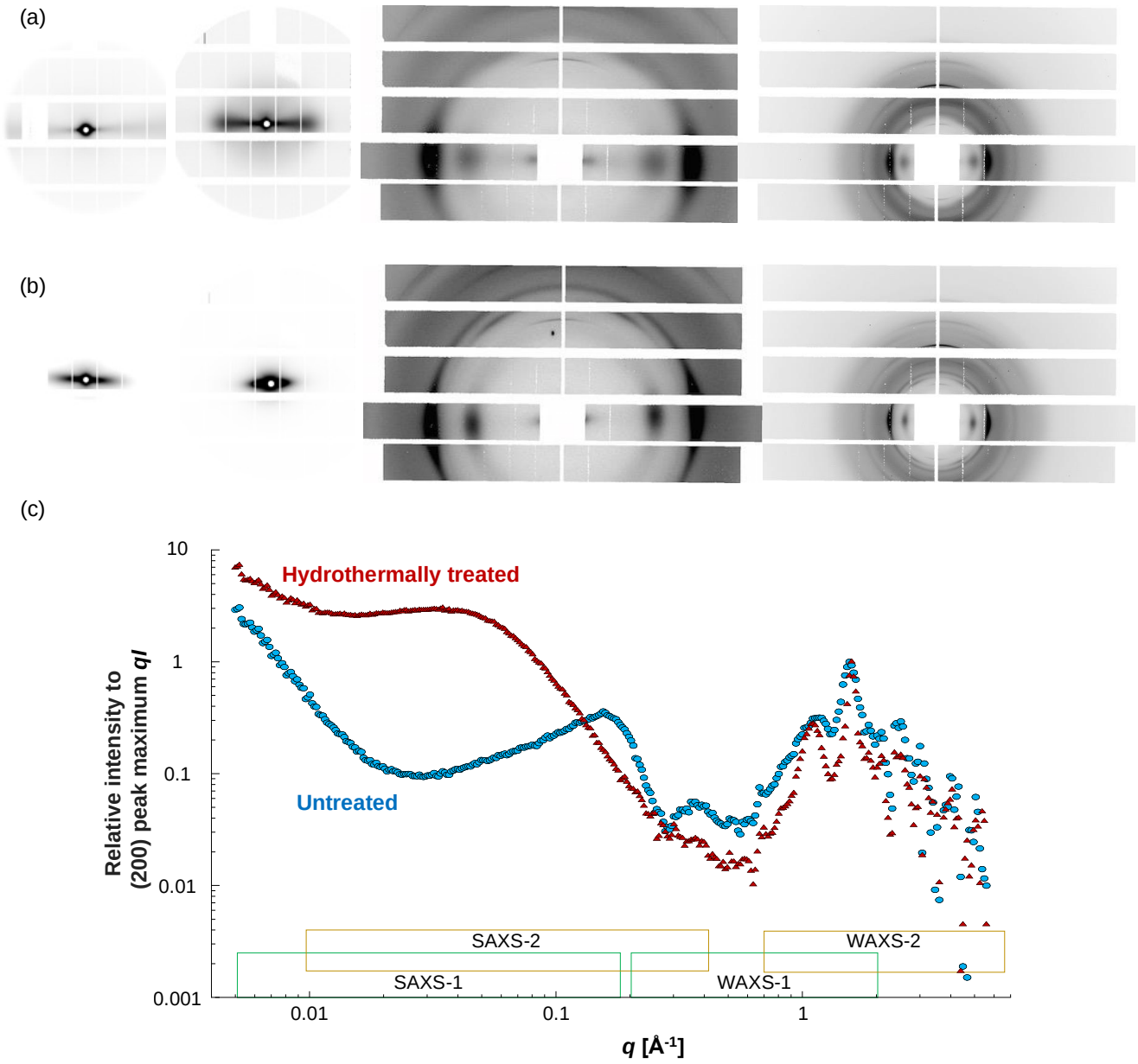

138 **Figure 1.** Two-dimensional scattering images (a, b) and profiles of equatorial
139 component (c) of the wet oak wood sample (*Quercus* sp.) before ((a) and blue profile in
140 (c)) and after hydrothermal treatment at 200 °C for 2 hours ((b) and red profile in (c)).
141 Scattering images in (a) and (b) are SAXS-1, SAXS-2, WAXS-1, and WAXS-2 from left
142 to right. The X-ray beam was irradiated orthogonal to the wood fiber direction (i.e., the
143 fiber direction was vertical in the diagrams).
144

In the WAXS range, a composite peak of 1 -1 0/1 1 0 reflections and the 2 0 0 reflections of cellulose Iβ are visible at 1.1 and 1.6 $Å^{-1}$, respectively. The pattern before the thermal treatment (blue profile) is typical of wood samples, and the positions and the intensity ratio roughly correspond to those obtained from highly crystalline cellulose Iβ. After hydrothermal treatment at 200°C, the equatorial reflections became much sharper due to the co-crystallization of microfibrils as reported previously (Fig. 1(a) and (b)) (Kuribayashi et al. 2016, 2019).

In the lower q range recorded, two peaks are present at q = 0.1 - 0.2 $Å^{-1}$ and q = 0.3 - 0.4 $Å^{-1}$ in the untreated sample (Fig. 1 (a)). Several studies have previously observed the former peak using X-ray (Jakob et al. 1996; Chen et al. 2021; Paajanen et al. 2022) or neutron (Fernandes et al. 2011; Nishiyama et al. 2014). The peak can be explained by the correlation between hard cylinders (i.e. cellulose microfibrils) randomly packed in the cell wall (Jakob et al. 1996) or the center-to-center distance of cylinders (Fernandes et al. 2011) or the convolution of the form factor of cylindrical microfibrils and their correlation (Chen et al. 2021). The latter peak has not been clearly explained, while Viljanen and co-workers (2020) reported a peak fitting of the peak observed in a SAXS profile of a tropical wood using a form factor of a cylinder. In Paajanen et al. (2022), the sample volume in the beam was probably too small compared to the Kapton window film whose scattering overlapped with this peak. In Jakob et al. (1996), the part of the peak can be recognized, but the limited q-range did not allow the appreciation of the whole feature. In our study, we used a sample thickness of about 2.5 mm, leading to sufficiently high scattering intensity with respect to the contribution of optical elements in the beam, revealing that this peak is another common scattering feature of many hardwood species.

The hydrothermal treatment drastically changed the scattering features: the 0.3 $Å^{-1}$ and the 0.15 $Å^{-1}$ peaks completely disappeared, and a new peak appeared at a much lower q range (0.01- 0.05$Å^{-1}$). The streak intensities increased in the q range of 0.06 - 0.6 $Å^{-1}$. Below q = 0.01 $Å^{-1}$, the intensity decay followed a power law. We carried out the same hydrothermal treatment on the 24 species. As summarized in Fig. 2, the small angle peaks (white arrowheads in Fig. 2(b)) were visible between 0.12 - 0.16 A^{-1} in most wood species before the treatment except 4 species *(D. kaki*, *C. sinensis*, *K. septemlobus*, and *S. japonicum*). Similar to the case of *Quercus* sp., this peak disappeared after the thermal treatment, and the new broad peak appeared centered 0.02 - 0.04 A^{-1} (black arrowheads in Fig. 2(b)). This change indicates that the hydrothermal treatment commonly induced the structural coarsening of approximately one order of magnitude in length scale in the cell walls of these 20 species.

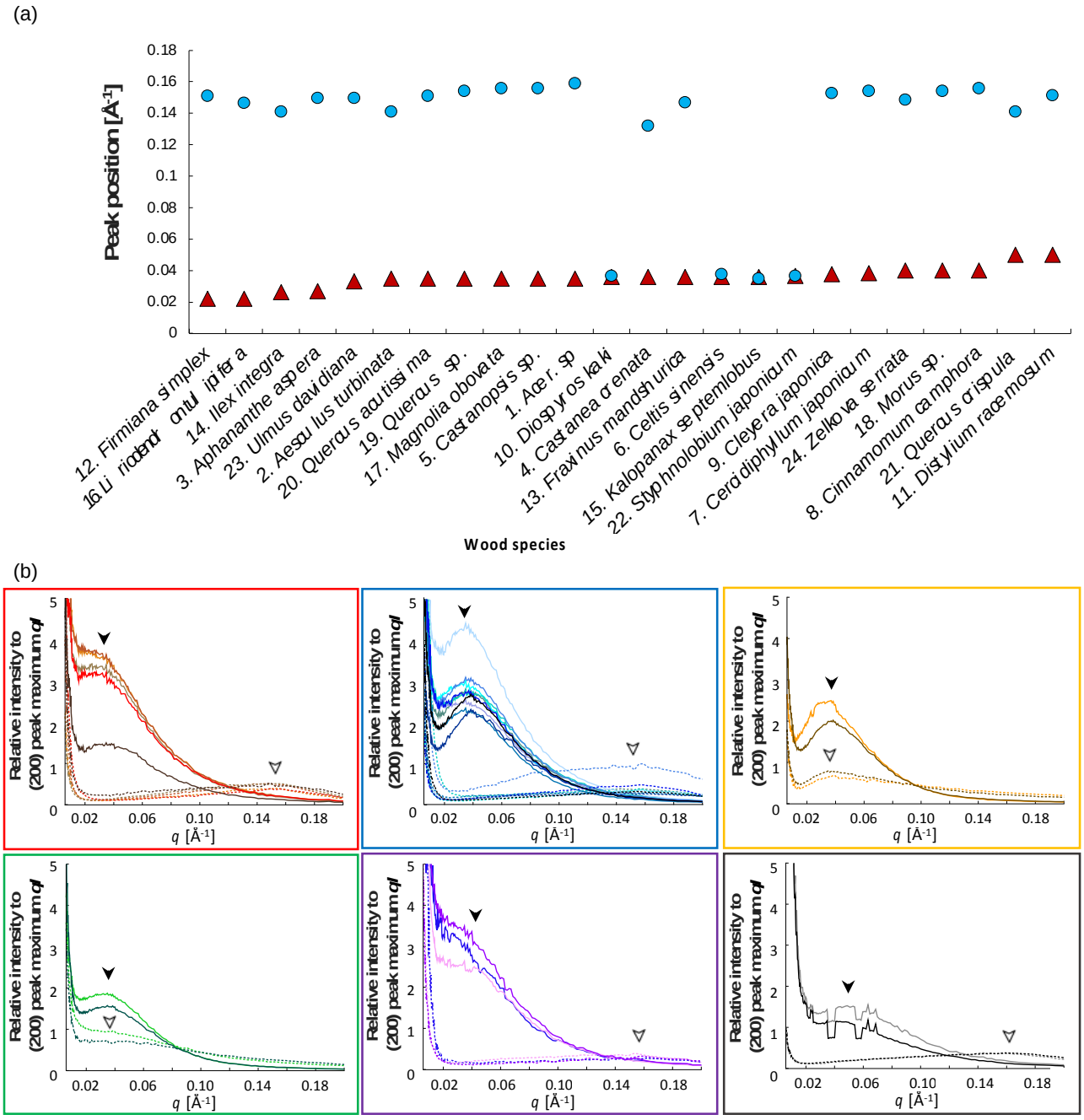

181 **Figure 2.** (a) Peak positions of prominent correlation peaks of 24 wood species before
182 (blue circle) and after the hydrothermal treatment (red triangle). (b) Corresponding X-
183 ray scattering profiles before (dotted lines) and after the hydrothermal treatment (solid
184 lines) in the double linear scale. The line colors in (b) correspond to those in (a).

185

186 On the other hand, the above-mentioned 4 species had small-angle peaks at 0.03 A^{-}

[1] before the hydrothermal treatment (Fig. 2(a)). While the peak intensities increased, the peak positions remained at the same positions after the treatment of these species (Fig. 2(b)). Thus, the hydrothermal treatment did not strongly affect the structural features at this ten-nanometer length scale related to the organization of cellulose microfibrils in the cell walls. Optical micrographs of *C. sinensis* (6), *K. septemlobus* (15) before the treatment show thick G-layers in the fiber cells (Fig. S1). The G-layer is a non-lignified cell wall layer composed mostly of cellulose. The lack of the matrix components in the G-layer may cause the coalescence of cellulose microfibrils, similarly in the hydrothermally treated cell walls, resulting in a coarse cell wall structure and hence similar scattering features before and after the treatment. The other two species, *D. kaki* (10), *S. japonicum* (22), as well as the remaining 22 specimens, did not show G-layer in their micrographs, while the scattering patterns were similar to the aforementioned species with the tension wood feature (Fig. S1). The solid-state ^{13}C NMR analysis suggested that specimens of *C. sinensis* (6), *K. septemlobus* (15), *D. kaki* (10) contained a higher amount of crystalline cellulose compared to other specimens (Kuribayashi, 2019).

Q range below 0.01Å^{-1}

In the smaller angle region below 0.01 A^{-1}, power-law behavior can be seen after hydrothermal treatment, as shown in Fig. 3. The straight line extends to q = 0.4 Å^{-1} in 21 species, as seen in the double logarithmic scale. The slope constants were between -1.3 to -1.5. The remaining 3 species, *D. racemosum* (11), *Morus* sp. (18), *Q. crispula* (21), show higher exponents in the low q range below 0.01 A^{-1}. In particular, the constants for *D. racemosum* and *Q. crispula* are -3, corresponding to the presence of a

clear interface in the structure. This might be due to air bubbles in the specimens,

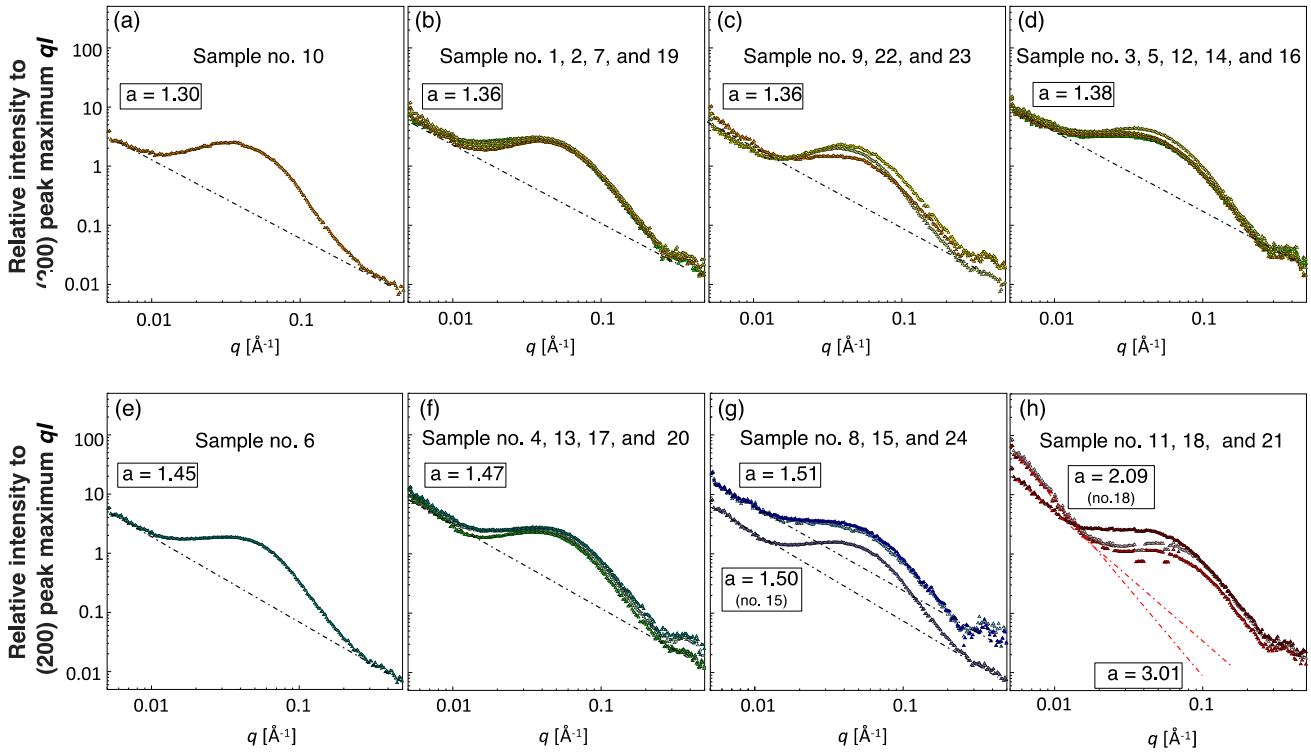

resulting in the air-solid interfaces.

Figure 3. Scattering profiles of 24 hydrothermally treated wood species between q = 0.006 and 0.3 $Å^{-1}$ in double log scale with power-law slopes as dotted lines (a). Numbers correspond to those in Table 1.

The relationship between the slope constants and the peak positions after the hydrothermal treatment is shown in Fig. 4. Among 24 species studied in this study, 17 of them show a notable similarity in these two scattering features in the small angle regions, with the power-low exponent of about -1.4 and the peak positions at 0.032 to 0.04 A^{-1}. Despite the taxonomical and ultrastructural differences found before the treatment, the hydrothermal treatment at 200 °C converges to a similar structure in the

cell wall at a nanometric length scale.

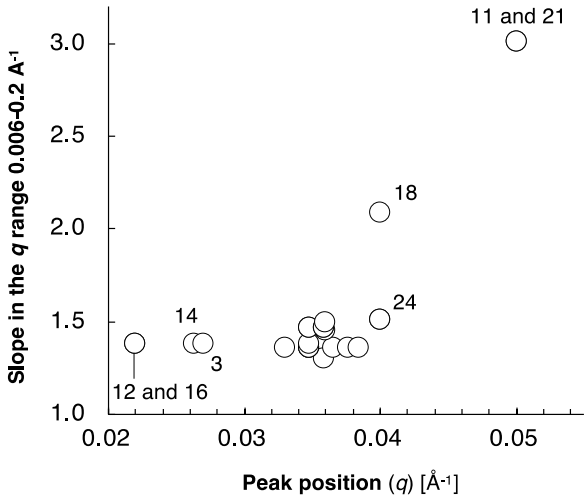

Figure 4. Relationship between power-law slope constants and peak positions of the main correlation peak of 24 wood species after hydrothermal treatment. Numbers correspond to those in Table 1.

Structural changes during the in-situ experiment

To follow the structural changes due to the hydrothermal treatment, we performed in situ S/WAXS measurements during the hydrothermal treatment of beech wood (*Fagus crenata*) at 200 °C, as shown in Fig. 5. This series of the equatorial scattering profiles indicates that these changes occurred only in the water-saturated sample but not in the air-dried sample (Fig. 5(a) and (b)). All the major structural changes happened during the heating process, and the cooling did not affect the structure. The increase in the streak intensity at $q < 0.2$ Å^{-1} started at 160 °C. Fig. S1(a)). The 0.3-Å^{-1} peak weakened and eventually disappeared during the heating from 130˚C to 150˚C. The 0.15-Å^{-1} peak also disappeared during the heating, where the intensity weakening started at around 160 ˚C. This temperature range of around 160 ˚C is typically the onset of autohydrolysis

of hemicelluloses (Santucci et al. 2015). Thus, the loss of the 0.15 $Å^{-1}$ peak may originate from the collapse of cellulose microfibrils induced by removing hemicelluloses from the interfibrillar space. This possible mechanism also explains the less pronounced structural change in the air-dried sample, as the extensive autohydrolysis requires excess water in the system.

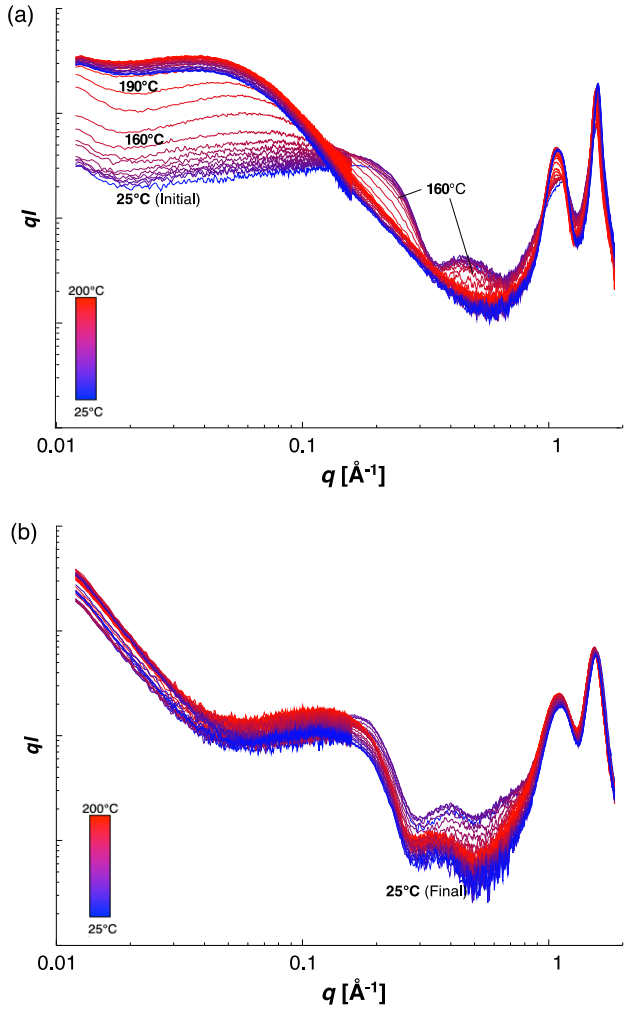

Figure 5. In situ S/WAXS profiles of the equatorial component during hydrothermal treatment. Green (a) and air-dry (b) beech wood (*F. crenata*).

Conclusion

Most hardwoods show similar equatorial scattering features that represent the structure in the cross-section of the cell wall, in the q range spanning 3 decades between 0.004 and 2 $Å^{-1}$. In a water-swollen native state, there is a prominent correlation peak between 0.1 and 0.2$Å^{-1}$ and a second peak between 0.2 and 0.4 $Å^{-1}$. These correlation peaks disappear upon hydrothermal treatment above 160˚C, accompanied by a buildup of a correlation peak in the 0.03 - 0.04 $Å^{-1}$ range. Some exceptions were seen in cellulose-rich samples, where the correlation peaks between 0.1 and 0.4 $Å^{-1}$ are absent in the native state. The hydrothermal treatment is probably leaching out the matrix component between the microfibrils leading to the collapse of microfibrils with each other in the normal wood. In contrast, cellulose microfibrils are already collapsed to each other in the native state in cellulose-rich cell walls.

Competing interests

The authors have no relevant financial or non-financial interests to disclose.

Consent for publication

All authors have provided their consent for publication.

Availability of data

All data generated or analyzed during this study are included in this article and the supporting information file.

Authors' contributions

T.K., Y.O., and Y.N. conceptualized the study. T.K., Y.O., I.M., and Y.N. performed the experiments. T.K., Y.O., and Y.N. analyzed the data. T.K., Y.O., and Y.N. wrote the manuscript. Y.M. and Y.N. supervised the study. All authors read and approved the final manuscript.

Acknowledgements and funding.

This study was supported by JSPS KAKENHI Grant Number JP17J05156 (T.K.). The dried wood specimens were obtained through collaborative research using wood collection databases with Research Institute for Sustainable Humanosphere (RISH) (Y.M. and T.K.). We thank Prof. Junji Sugiyama and Hajime Sorimachi (Kyoto University, Japan) for advising us on the selection of wood specimens. We thank the support of Prof. Yukie Saito (The University of Tokyo, Japan) and The University of Tokyo Chichibu Forest and Arboricultural Research Institute (UTCF) during the sampling of beech green wood specimens. We acknowledge Glyco@Alps (ANR-15-IDEX-02) for the financial support. The wide-angle X-ray detector (WOS) was funded by the French National Research Agency (ANR) under the 'Investissement d'Avenir' program (Grant No. ANR-11-EQPX-0010). ESRF is acknowledged for the provision of beamtimes (experiment numbers A02-1-892 and A02-1-864, D2AM beamline).

Ethics approval and consent to participate

Not applicable.

References

291 Ashiotis G, Deschildre A, Nawaz Z, et al (2015) The fast azimuthal integration Python
292 library: pyFAI J Appl Crystallogr 48:510–519.
293 https://doi.org/10.1107/S1600576715004306
294 Chen P, Li Y, Nishiyama Y, et al (2021) Small Angle Neutron Scattering Shows
295 Nanoscale PMMA Distribution in Transparent Wood Biocomposites. Nano Lett
296 21:2883–2890. https://doi.org/10.1021/acs.nanolett.0c05038
297 Driemeier C, Mendes FM, Santucci BS, Pimenta MTB (2015) Cellulose co-
298 crystallization and related phenomena occurring in hydrothermal treatment of
299 sugarcane bagasse. Cellulose 22:2183–2195. https://doi.org/10.1007/s10570-015-
300 0638-7
301 Fernandes AN, Thomas LH, Altaner CM, et al (2011) Nanostructure of cellulose
302 microfibrils in spruce wood. Proc Natl Acad Sci 108:E1195–E1203.
303 https://doi.org/10.1073/pnas.1108942108
304 Garrote G, Domínguez H, Parajó JC (1999) Hydrothermal processing of lignocellulosic
305 materials. Holz als Roh - und Werkst 57:191–202.
306 https://doi.org/10.1007/s001070050039

307 Jakob HF, Fratzl P, Tschegg SE (1994) Size and Arrangement of Elementary Cellulose
308 Fibrils in Wood Cells: A Small-Angle X-Ray Scattering Study of Picea abies. J
309 Struct Biol 113:13–22. https://doi.org/https://doi.org/10.1006/jsbi.1994.1028
310 Jakob HF, Tschegg SE, Fratzl P (1996) Hydration Dependence of the Wood-Cell Wall
311 Structure in Picea abies. A Small-Angle X-ray Scattering Study. Macromolecules
312 29:8435–8440. https://doi.org/10.1021/ma9605661
313 Kocaefe D, Huang X, Kocaefe Y (2015) Dimensional stabilization of wood. Curr For
314 Reports 1:151–161. https://doi.org/10.1007/s40725-015-0017-5
315 Kuribayashi T, Ogawa Y, Rochas C, et al (2016) Hydrothermal Transformation of
316 Wood Cellulose Crystals into Pseudo-Orthorhombic Structure by Cocrystallization.
317 ACS Macro Lett 5:730–734. https://doi.org/10.1021/acsmacrolett.6b00273
318 Kuribayashi, T., Ogawa, Y., Matsumoto, et al (2019). Changes in Crystal Structure of
319 Cellulose in Hardwood Cell Walls by Hydrothermal Treatment at 200 °C under 1.6
320 Mpa. Mokuzai Gakkaishi, 65:212-217.
321 Nishiyama Y, Langan P, O'Neill H, et al (2014) Structural coarsening of aspen wood by
322 hydrothermal pretreatment monitored by small- and wide-angle scattering of X-
323 rays and neutrons on oriented specimens. Cellulose 21:1015–1024.
324 https://doi.org/10.1007/s10570-013-0069-2

325 Nitsos CK, Matis KA, Triantafyllidis KS (2013) Optimization of hydrothermal
326 pretreatment of lignocellulosic biomass in the bioethanol production process.
327 ChemSusChem 6:110–122. https://doi.org/10.1002/cssc.201200546
328 Nitsos CK, Choli-Papadopoulou T, Matis KA, Triantafyllidis KS (2016) Optimization
329 of hydrothermal pretreatment of hardwood and softwood lignocellulosic residues
330 for selective hemicellulose recovery and improved cellulose enzymatic hydrolysis.
331 ACS Sustain Chem Eng 4:4529–4544.
332 https://doi.org/10.1021/acssuschemeng.6b00535
333 Paajanen A, Zitting A, Rautkari L, et al (2022) Nanoscale Mechanism of Moisture-
334 Induced Swelling in Wood Microfibril Bundles. Nano Lett 22:5143–5150.
335 https://doi.org/10.1021/acs.nanolett.2c00822
336 Penttilä PA, Rautkari L, Österberg M, Schweins R (2019) Small-angle scattering model
337 for efficient characterization of wood nanostructure and moisture behaviour. J
338 Appl Crystallogr 52:369–377. https://doi.org/10.1107/S1600576719002012
339 Romaní A, Garrote G, Alonso JL, Parajó JC (2010) Bioethanol production from
340 hydrothermally pretreated Eucalyptus globulus wood. Bioresour Technol
341 101:8706–8712. https://doi.org/10.1016/j.biortech.2010.06.093

342 Sandberg D, Kutnar A (2016) Thermally modified timber: Recent developments in
343 Europe and North America Wood Fiber Sci 48:28–39
344 Santucci BS, Maziero P, Rabelo SC, et al (2015) Autohydrolysis of Hemicelluloses
345 from Sugarcane Bagasse During Hydrothermal Pretreatment: a Kinetic Assessment.
346 BioEnergy Res 8:1778–1787. https://doi.org/10.1007/s12155-015-9632-z
347 Viljanen M, Ahvenainen P, Penttilä P, Svedström K. (2020) Ultrastructural X-ray
348 scattering studies of tropical and temperate hardwoods used as tonewoods. IAWA
349 J., 41:301–319. https://doi.org/10.1163/22941932-bja10010
350 Wojtasz-Mucha J, Hasani M, Theliander H (2017) Hydrothermal pretreatment of wood
351 by mild steam explosion and hot water extraction. Bioresour Technol 241:120–126.
352 https://doi.org/10.1016/j.biortech.2017.05.061
353